Chinese Chemical Letters 35 (2024) 109187

Contents lists available at ScienceDirect

Chinese Chemical Letters

journal homepage: www.elsevier.com/locate/cclet

Active molecule-based theranostic agents for tumor vasculature normalization and antitumor efficacy

Jin Wang[a,1], Xiaoyan Pan[a,1], Junyu Zhang[a], Qingqing Zhang[a], Yanchen Li[a], Weiwei Guo[b,*], Jie Zhang[a,*]

[a] School of Pharmacy, Health Science Center, Xi'an Jiaotong University, Xi'an 710061, China
[b] Center of Advanced Pharmaceuticals and Biomaterials, State Key Laboratory of Natural Medicine, China Pharmaceutical University, Nanjing 210009, China

ARTICLE INFO

Article history:
Received 11 August 2023
Revised 4 October 2023
Accepted 6 October 2023
Available online 14 October 2023

Keywords:
Tumor vasculature normalization
Diagnosis and treatment
Cytotoxicity
Depleting glutathione
Ferroptosis
Immune activation

ABSTRACT

Tumor vascular normalization has emerged as a promising strategy for synergistic therapy recently. Based on the strategy of "fluorescence turn on-controllable release", a novel bifunctional candidate was constructed based on previous developed vascular normalization inducer QDAU5, which could self-assemble to form functional enzyme infrared QDAU5 nanoparticles (FEIRQ NPs). Subsequently, biological evaluation demonstrated that the FEIRQ NPs could induce ferroptosis, endoplasmic reticulum stress, and antigen preconditioning and maturation of dendritic cells and $CD8^+$ T cells, leading to excellent antitumor efficacy in the absence of cytotoxic drugs. Additionally, FEIRQ NPs show high fluorescence intensity upon exposure to the β-galactosidase (β-Gal) enzyme expressed in ovarian cancer, enabling real-time monitoring of therapeutic effects. Overall, our findings suggest a prospering strategy to early diagnosis and efficient therapy for ovarian cancer without cytotoxicity.

Tumor vascular normalization has emerged as a promising strategy for synergistic therapy in recent years. Normalization of tumor vascular can alleviate tumor hypoxia microenvironment, reduce malignancy and improve the efficacy of conventional treatment [1,2]. Vascular normalization could reshape tumor microenvironment and enhance the efficacy of radiotherapy, targeted therapy, immunotherapy, reversing drug resistance, and inhibiting tumor invasion and metastasis [3,4]. However, the evidences from preclinical and initial clinical trials demonstrated the existence of a narrow normalization "time window" which is difficult to accurately monitor in real time. Moreover, it was found that vascular normalization inducers are not effective when administered alone and need to be combined with cytotoxic drugs within the vascular normalization time window to exert efficient synergistic antitumor effects [5,6]. Unfortunately, the time window of vascular normalization cannot be precisely controlled, which may result in inefficient antitumor effects when drugs are combined [7]. Therefore, there is an urgent need to find a means that induce vascular normalization while exerting efficient antitumor effects alone without being limited by the vascular normalization time window.

Ovarian cancer is a deadly disease that affects more than 220,000 women worldwide each year [8–10]. It is known as the "silent killer" because there are no obvious symptoms in the early stages, making it easily missed [11–13]. Chemotherapy is the classical treatment for ovarian cancer [14]. The treatment modality for advanced ovarian cancer is mainly platinum-based first-line chemotherapy, which can provide temporary remission for a significant proportion of patients with advanced ovarian cancer, but about 70% of advanced patients may still have recurrence [15]. Some angiogenesis inhibitors have been used in combination with cytotoxic drugs treatment to achieve better anti-tumor effects in ovarian cancer. This is since such angiogenesis inhibitors (vascular normalization inducers) combine with cytotoxic drugs while inducing vascular normalization to exert efficient anti-ovarian cancer effects [16]. However, cytotoxic drugs are characterized by high toxicity and poor pharmacokinetics, which significantly affect the life quality of patients. Therefore, it is urgent to develop a novel, low toxicity method for early diagnosis and efficient treatment for ovarian cancer.

β-Galactosidase (β-Gal) is a glycoside hydrolase that hydrolyzes the β-glycosidic bond formed by galactose and other molecules [17–21]. Recently, β-Gal has been widely recognized as an important biomarker of overexpression in ovarian cancer [22–24]. β-Gal enzyme is significantly expressed in ovarian cancer cells (SKOV3 cells). Therefore, fluorescent probes to visualize β-Gal

* Corresponding authors.
E-mail addresses: guoweiwei@cpu.edu.cn (W. Guo), zhj8623@mail.xjtu.edu.cn (J. Zhang).
[1] These authors contributed equally to this work.

https://doi.org/10.1016/j.cclet.2023.109187
1001-8417/

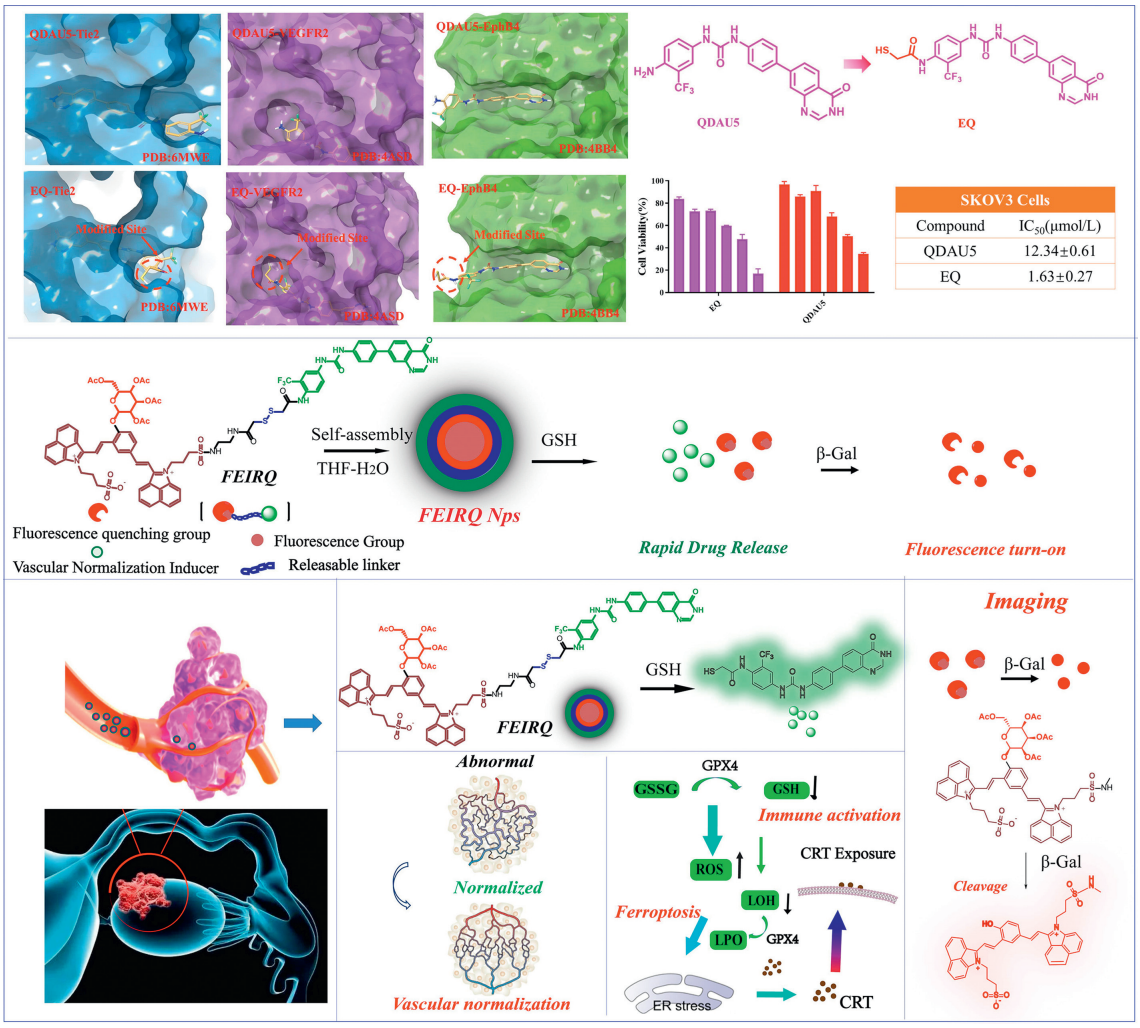

Fig. 1. Schematic representation of imaging and treatment for tumor.

can be designed for early diagnosis and treatment of ovarian cancer.

We previously developed a potent drug candidate, QDAU5, for inducing vascular normalization (Fig. 1) [25]. However, *in vitro* experiments showed that QDAU5 still required the involvement of cytotoxins to reduce tumor volume [26]. Subsequently, we carried out further optimization affording a novel active molecule (EQ) which showed significantly increased anti-ovarian cancer activity (Figs. S1 and S3 in Supporting information). However, due to the instability of the sulfhydryl group and the need for efficient antitumor effects as well as real-time monitoring, we further optimized the structure of EQ by conjugating a caged near-infrared fluorophore to generate a novel bifunctional prodrug, FEIRQ (Scheme S1 in Supporting information). The structure was constructed by ^{1}H nuclear magnetic resonance (NMR) and ^{13}C NMR (Figs. S10–S13 in Supporting information). FEIRQ is an amphiphilic molecule which could rapidly self-assemble into nanoparticles (FEIRQ NPs) under physiological conditions. FEIRQ NPs is stable in the systemic circulation but will be degraded in the tumor microenvironment, where the disulfide linkage in FEIRQ is sensitive to the high concentration of glutathione (GSH) in the microenvironment. At the same time, β-Gal hydrolyzes the pyranogalactoside bond to decage the fluorescence for real-time *in vivo* monitoring of ovarian cancer. Its rupture releases EQ to induce vascular normalization and deplete GSH to induce ferroptosis (Fig. S6 in Supporting information). Moreover, FEIRQ NPs can indirectly activate the immune system and exert an efficient anti-ovarian cancer effect without the need for monitoring the vascular normalization time window or combination with cytotoxic drugs.

Due to the large molecular weight of FEIRQ, its pharmacokinetic properties are greatly affected. Considering the existence of hydrophilic and hydrophobic groups, self-assembly facilitates their formation into nanoparticles with the expectation of improving their pharmacokinetic properties. The self-assembled nanoparticle formation was carried out in tetrahydrofuran (THF) without an additional catalyst, and was completed within 5 min at room temperature [27]. The FEIRQ NPs were prepared by self-assembly in THF-H_2O, and the particle size of FEIRQ NPs determined by dynamic laser scattering (DLS) is 38.5 nm with a narrow distribution. In addition, the FEIRQ NPs solution exhibits a typical brightness of nanomorphs (Fig. S4a in Supporting information). The clear spherical morphology was visualized by transmission electron microscopy (TEM), with round regular structures (Fig. S4b in Supporting information). In addition, FEIRQ NPs shown excellent storage stability at 4 °C for at least 50 days (Fig. S4c in Supporting information). The outstanding stability typically indicated that the functional molecules do not degrade spontaneously, which is the main factor for maintaining the activity of the FEIRQ NPs. Next, it is essential to vertify the *in vivo* release of the drug. The results showed that the particle size increased sharply under GSH (10 mmol/L, acetate buffer solution (ABS)), which could be disassembled and release EQ. In addition, we also explored the release conditions by

TEM in the tumor microenvironment (10 mmol/L GSH, ABS), which showed that EQ was released from FEIRQ under GSH (10 mmol/L) (Figs. S4d and S9 in Supporting information). As a result, the tumor microenvironment triggered the disassembly of FEIRQ NPs, and EQ was also released from the functional FEIRQ NPs.

The optical properties of FEIRQ NPs were measured in a mixture of phosphate buffered saline/dimethyl sulfoxide (PBS/DMSO; v/v = 8:2, 2 μmol/L). As described in Fig. S4e (Supporting information), FEIRQ NPs exhibited a broad absorption spectrum from 400 nm to 650 nm in aqueous media, with a maximum absorption peak of 525 nm. The fluorescence spectra show that FEIRQ NPs has almost no fluorescence signal in the mixture. To investigate the response and efficiency of FEIRQ NPs to β-Gal, the optical properties of FEIRQ NPs were studied in the presence of β-Gal. After incubation with β-Gal (5 units) for 30 min, the fluorescence intensity of FEIRQ NPs at 560 nm decreased, while the fluorescence intensity at around 706 nm increased with concentration (Figs. S4f and g in Supporting information). Subsequently, the specificity of the fluorescence spotting of FEIRQ NPs was evaluated for different analytes, including cations, reduced anions, reactive oxygen species, amino acids and various enzymes, measured by fluorescence spectroscopy after incubation with FEIRQ NPs (2 μg/mL) for 30 min. The results are shown in Figs. S4h–j (Supporting information). There is an increase in fluorescence intensity of FEIRQ NPs only for analytes other than β-gal, while the presence of the remaining analytes does not illuminate the fluorescence signal. This indicates that FEIRQ NPs exhibits specific selectivity for β-gal under physiological conditions.

Next, we simulated a highly reduced tumor microenvironment (10 mmol/L GSH) *in vitro* and validated the release characteristics and release mechanism of FEIRQ NPs by HPLC and mass spectrometry. As we expected, FEIRQ achieved 80% stable release under tumor microenvironment conditions for 40 h (Fig. S4k in Supporting information). In addition, the release system of intracellular FEIRQ was detected by mass spectrometry and the remaining FEIRQ and key release intermediates such as EQ could be detected (Figs. S4j and l in Supporting information). All these results suggest that FEIRQ breaks disulfide bonds in the presence of GSH and releases EQ active molecules to play a regulatory role.

To ensure that FEIRQ NPs can be applied for subsequent in-depth imaging and therapeutic analysis. Previously restricted analysis of the cytotoxicity of FEIRQ NPs was performed. The cytotoxicity of FEIRQ and FEIRQ NPs were observed in normal cells (HEK293) (Fig. S2 in Supporting information). Even at high concentrations of FEIRQ NPs of 100 μg/mL, HEK293 cells maintained a high survival rate of more than 80% after 48 h. After confirming the low cytotoxicity of FEIRQ NPs, we verified its fluorescence spotting and labeling properties at the cellular level. As FEIRQ NPs was constructed based on the lighting of β-Gal, we selected FEIRQ NPs for cell imaging analysis on cells with high expression of β-Gal (SKOV3 cells) and cells with high expression of β-Gal (EA. hy926 cells) (Figs. S5a and b in Supporting information). Consistent with our assumptions, FEIRQ NPs could achieve fluorescent labeling for endogenous β-Gal cells (SKOV3 cells) and not achieve labeling for normal cells (EA. hy926). To be excited, the FEIRQ NPs showed excellent cell labeling compared with FEIRQ. Moreover, cell uptake experiments also verified that FEIRQ NPs could achieve specific fluorescent lighting *in vitro* (Fig. S5c in Supporting information).

It was found that FEIRQ and FEIRQ NPs can directly deplete GSH through disulfide bond cleavage, thereby increasing the reactive oxygen species (ROS) level of tumor cell injury. Then, to further clarify that functional molecules and nanoparticles could enhance ferroptosis and immunity through the combined effect of EQ and disulfide bonds, we investigated the relevant indicators of ferroptosis and immune activation induced by EQ, azo compounds alone, FEIRL, and combinations of these molecules. Free EQ produced weak tumor growth inhibition, and cytostatic effects remained weak at 43.4% after free EQ treatment, and all other treatments had weak effects on growth inhibition (Fig. S1). Nevertheless, FEIRQ and FEIRQ NPs showed potent tumor cell inhibition. Cell viability was all nearly retained in HEK293 (normal cells) compared with the blank group, reflecting the low cytotoxicity of FEIRQ NPs (Fig. S5d in Supporting information). Meanwhile, cell inhibition (Figs. S5e and f in Supporting information), cell migration (Figs. S5g and h in Supporting information), apoptosis (Figs. S5i and j in Supporting information), and cell cycle (Figs. S5k and l in Supporting information) were all improved in SKOV3 cells compared with the blank group, reflecting the outstanding preliminary antitumor effects of FEIRQ and FEIRQ NPs. Notably, the cleavage of disulfide bonds will certainly deplete GSH. intracellular GSH levels decreased to 29.81% after FEIRQ NPs treatment compared to the control group (Fig. 2a), while only to 68.80% after EQ-only treatment. Disulfide bonding alone did not cause depletion of GSH. It was further confirmed that the presence of EQ and disulfide bonds in the FEIRQ NPs had a synergistic effect in depleting GSH. Furthermore, the upregulation of lipid peroxidation (LPO) levels in SKOV3 cells confirmed ferroptosis (Fig. 2b). Accordingly, FEIRQ and FEIRQ NPs induce oxidative stress and release ROS in SKOV3 cells by depleting GSH. Therefore, we first assessed the intracellular GSH content. Intracellular ROS were detected by dichlorodihydro fluorescein diacetate (DCFH-DA) (Figs. 2c and d). In addition, the production of ROS, which could further induce the production of lipid oxidation. The upregulation of LPO levels in SKOV3 cells also confirmed ferroptosis. Based on this, we analyzed the levels of key proteins for ferroptosis. As is shown in Figs. 2e and f, the expression level of glutathione peroxidase 4 (GPX4) was significantly downregulated after FEIRQ NPs treatment. Meanwhile, the expression level of acyl-CoA synthase long chain family member 4 (ACSL4) was significantly upregulated. All of all, these results indicated that FEIRQ NPs could effectively induce ferroptosis in ovarian cancer cells (SKOV3 cells).

Ferroptosis leads to endoplasmic reticulum (ER) stress, releasing calreticulin, promoting antigen presentation and inducing immunogenic cell death (ICD) for immune activation [28]. To further verify the correlation between iron death and immune activation, we examined iron death as well as immune activation indicators. First, the occurrence of ER stress was not verified, and we analyzed for Bip, a key protein of ER stress, as well as C/EBP-homologous protein (CHOP). The results are shown in Figs. 2e and f, where the expression levels of Bip and CHOP were significantly upregulated after FEIRQ and FEIRQ NPs treatment, confirming the occurrence of ER stress in tumor cells. The generation of ER stress further promotes the release of calmodulin (CRT), which promotes antigen presentation and activates the immune system. The strong induction of ICD by FEIRQ NPs further promotes the maturation of dendritic cell (DC). In turn, DC2.4 cells, one of the most important types of antigen presenting cells (APCs), can promote their maturation. APCs play an important role in cancer immunotherapy. Therefore, the maturation of DC cells was analyzed. The results are shown in Figs. 2g and h, in which the maturation of DCs in the FEIRQ NPs group was as high as 18.27%, much higher than that in the FEIRQ group (9.27%), EQ (6.38%), mixed group (2.60%), and blank group (2.80%), confirming that FEIRQ NPs can indeed promote ER stress by inducing ferroptosis, releasing calreticulin, and promoting antigen presentation, and activating the immune system to exert anti-ovarian cancer effects.

FEIRQ and FEIRQ NPs exhibited excellent tumor cell killing potency and immune activation. We then further investigated the efficacy of the ID8 tumor model. Animal welfare and experimental procedures have been reviewed and approved by the Animal Ethics Committee of Xi'an Jiaotong University. The treatment regimen is shown in Fig. 3a, with FEIRQ and FEIRQ NPs administered by in-

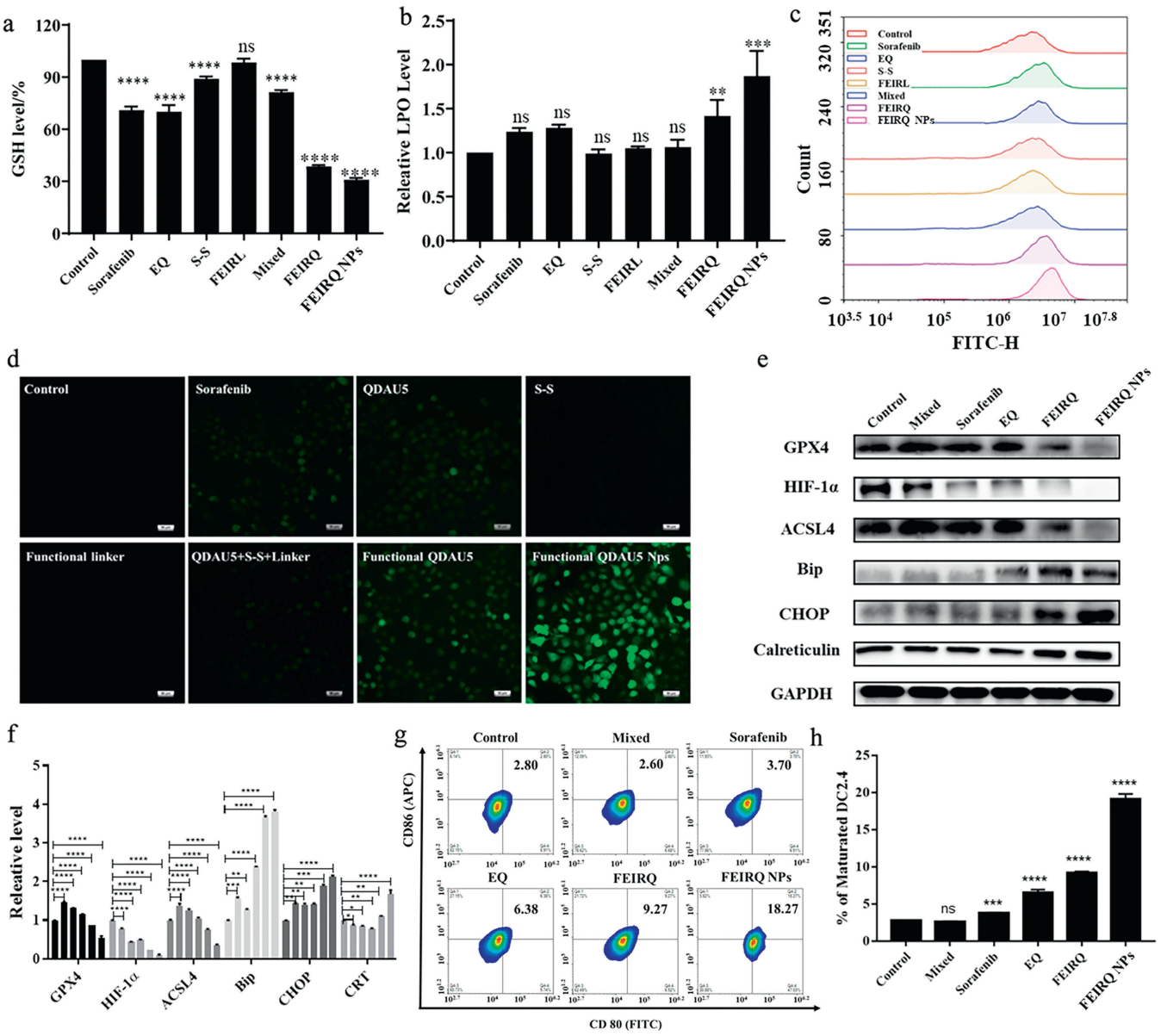

Fig. 2. (a) Intracellular GSH levels after different treatments. (b) The detection of LPO level in SKOV3 cells. (c) Cell uptake to detect ROS in SKOV3 cells. (d) Fluorescence ROS images of SKOV3 cells. Scale bar: 50 μm. (e, f) The expression level of GPX4, ACSL4, Bip, and CHOP in SKOV3 cells. (g, h) CRT exposure of SKOV3 cells after treatment with Mixed (EQ+FEIRL+S-S), sorafenib (ferroptosis inducer), EQ, FEIRQ and FEIRQ NPs (mean ± standard deviation (SD), *t*-test, compared to control groups; $^{*}P < 0.1$, $^{**}P < 0.01$, $^{***}P < 0.001$, $^{****}P < 0.0001$, $n = 3$).

travenous injection on days 0, 2, 4, 6, 8 and 12 for a total of 5 doses. The results showed that the FEIRQ and FEIRQ NPs have excellent biosafety and antitumor activity. As shown in Fig. 3g, no significant weight loss, histopathological damage, or death was observed, suggesting that the toxicity of FEIRQ and FEIRQ NPs was negligible (Fig. S7 in Supporting information). In addition, the tumors in the blank group grew rapidly and were 10 times larger than day 0. It was found that treatment with EQ and FEIRQ could not achieve satisfactory therapeutic effects (Fig. 3f). In contrast, FEIRQ NPs could significantly inhibit tumor growth and even led to partial tumor ablation, showing outstanding anti-ovarian tumor efficacy. Fig. 3e shows the tumors after stripping for each group, with the FEIRQ NPs group having much smaller tumor volumes than the mice treated with EQ and FEIRQ, and even disappearing. In addition, no mice died within 30 days and there was no significant damage to various tissues and organs. Overall, FEIRQ NPs showed superior anti-tumor efficacy and high biosafety *in vivo*.

Subsequently, we evaluated the effect on ferroptosis including GSH deficiency (Fig. 3c), LPO upregulation (Fig. 3d), and GPX4 downregulation (Fig. 3b) *in vivo*. The results showed that FEIRQ NPs could effectively induce ferroptosis. Otherwise, we analyzed the immune activation on day 12 after the first injection. As shown in Figs. 3h and i, the proportion of $CD8^+$ T cells infiltrating the tumor in the blank group was only 7.56%. The EQ (22.15%) and FEIRQ (28.23%) showed only a weak immune response. To be delighted, FEIRQ NPs could significantly improve immune activation and promoted $CD8^+$ T-cell infiltration to 43.03% in tumor tissue. This result confirmed that FEIRQ NPs could effectively increase immune activation in the tumor compared with EQ and FEIRQ. In addition, the ratio of $CD80^+$ cells to $CD86^+$ cells were analyzed by flow cytometry and used to assess the maturity of DCs in lymph nodes (LNs). As expected, FEIRQ NPs also induced the highest percentage of DC maturation to 43.43% (Figs. 3j and k). Overall, these results indicated that FEIRQ NPs exhibited strong

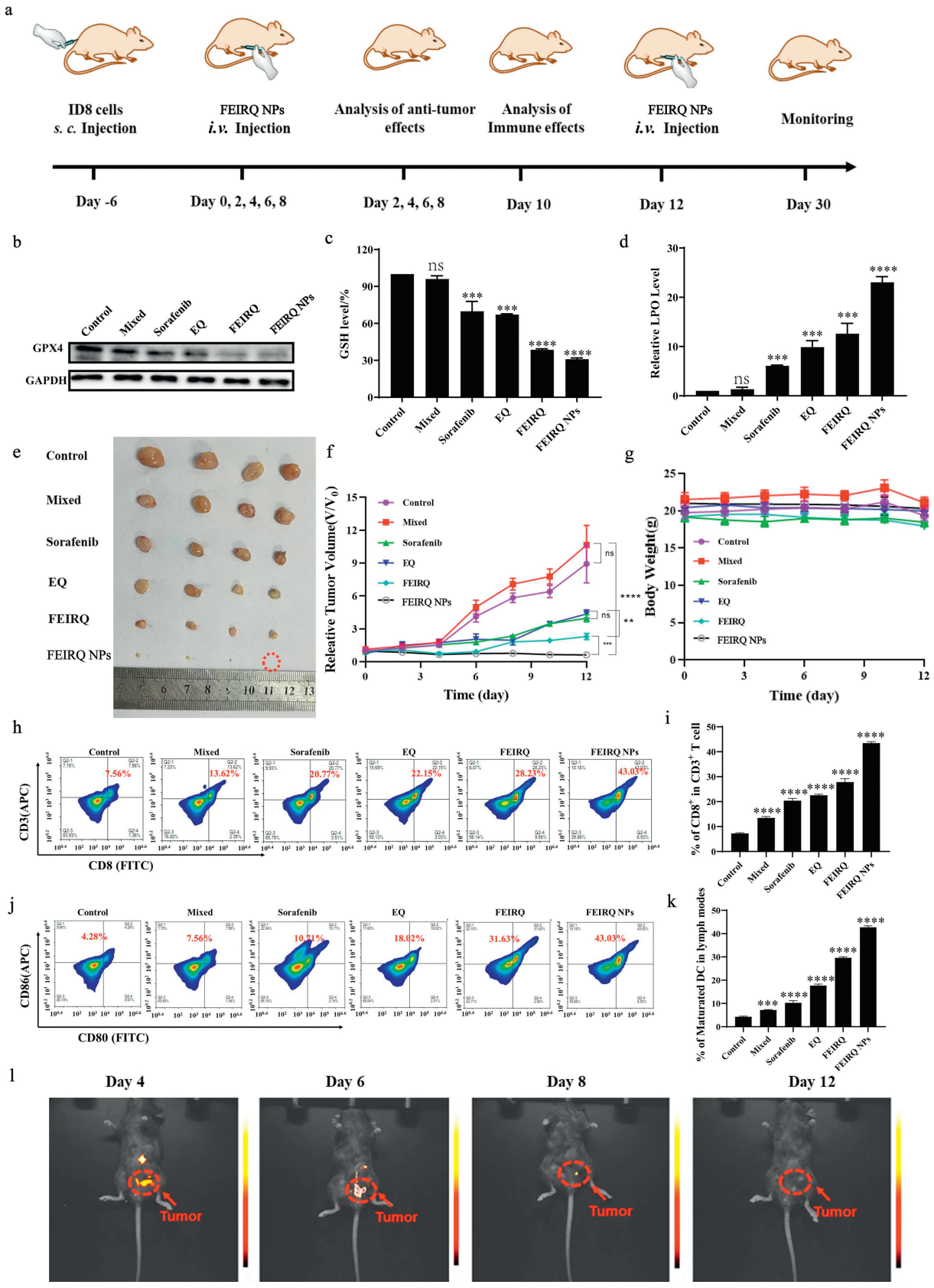

Fig. 3. (a) The treatment schedule of FEIRQ NPs. (b) Western blot analysis of GPX4 expression *in vivo*. (c) Tumor growth curve of the ID8 model. (d) The GSH level after different treatments *in vivo*. (e) The LPO level after different treatments *in vivo*. (f) Images of *ex vivo* tumors on day 12. (g) The body weight curve of the ID8 model. (h, i) The infiltration of $CD8^+$ T cells in tumors. (g, k) DC maturation in lymph nodes on day 10. (l) Fluorescence imaging *in vivo* (mean ± SD, *t*-test, compared to control groups; no significance (ns). $^*P < 0.1$, $^{**}P < 0.01$, $^{***}P < 0.001$, $^{****}P < 0.0001$, $n = 3$).

ferroptosis-inducing and immune-activating effects in ovarian cancer. Most importantly, the imaging *in vivo* showed that the fluorescence intensity was significantly weakened, and the tumor volume was reduced after the eighth day of treatment (Fig. 3l). In addition, FEIRQ NPs were mainly distributed in tumors and liver, which could further confirm that FEIRQ Nps have certain tumor targeting properties (Fig. S8 in Supporting information).

In summary, we developed a bifunctional molecule, FEIRQ, which was constructed based on a novel vascular normalization inducer developed in our study. It was incorporated with a disulfide bond and an NIR fluorophore of the cyanine backbone for the sensitive detection of β-Gal. Fortunately, those date indicated that the bifunctional molecule could self-assemble to form a nanoparticle and exhibited efficient labeling and antitumor effects in ovarian cancer. In the case of high expression of the β-Gal enzyme in ovarian cancer, FEIRQ NPs can be fluorescently illuminated to monitor the inhibitory potency against ovarian cancer. Meanwhile, under the action of EQ and disulfide bonds, the novel FEIRQ NPs could deplete GSH *in vivo*, as well as induce ferroptosis. Subsequently, it could indirectly activate the immune system, promote antigen presentation, and exert a highly effective antitumor potency without cytotoxic drugs. As we expected, FEIRQ NPs exhibited promising efficiency in imaging of ovarian cancer *in vivo* while displayed a significant antitumor effect. Overall, a novel bifunctional FEIRQ NPs with outstanding potency in integration of diagnosis and treatment was developed, which further confirmed that the strategy of "fluorescence turn on-controllable release" is reliable to construct bifunctional molecules with potency of both vascular normalization and visualization. FEIRQ NPs represents a promising therapeutic agent for the treatment of ovarian cancer without cytotoxic drugs, with the potential for real-time monitoring, vascular normalization, ferroptosis induction, and immune system activation. Our findings provided an effective strategy for early diagnosis and efficient treatment of ovarian cancer.

Declaration of competing interest

The authors declare that they have no known competing financial interests or personal relationships that could have appeared to influence the work reported in this paper.

Acknowledgments

This work was supported by the National Natural Science Foundation of China (NSFC, Nos. 82373793 and 82173742), the Science Fund for Distinguished Young Scholars of Shaanxi Province (No. 2022JC-54), and the Key Research and Development Program of Shaanxi Province (No. 2023-YBSF-131).

Supplementary materials

Supplementary material associated with this article can be found, in the online version, at doi:10.1016/j.cclet.2023.109187.

References

[1] S.F. Wen, K. Zhang, Y. Li, et al., Chin. Chem. Lett. 31 (2020) 3153–3157.
[2] S. Luo, C. Liang, Q. Zhang, P. Zhang, Chin. Chem. Lett. 34 (2023) 107666.
[3] G.S. Xie, L. Zhu, Y.Y. Song, et al., Chin. Chem. Lett. 32 (2021) 2164–2168.
[4] Y.L. Song, H.Q. Jing, L.B. Vong, et al., Chin. Chem. Lett. 33 (2022) 1705–1717.
[5] Y. Huang, B.Y.S. Kim, C.K. Chan, et al., Nat. Rev. Immunol. 18 (2018) 195–203.
[6] J. Ma, D.J. Waxman, Mol. Cancer Ther. 7 (2008) 3670–3684.
[7] W. Li, Y.Y. Quan, Y. Li, et al., Cancer Manag. Res. 10 (2018) 4163–4172.
[8] M. Chen, Y. Xie, Q. Luo, et al., Chin. Chem. Lett. 34 (2023) 107744.
[9] C. Yang, B.R. Xia, Z.C. Zhang, et al., Front. Immunol. 11 (2020) 77869.
[10] J. Rais, A. Jafri, S. Siddiqui, et al., Front. Biosci. 9 (2017) 67–75.
[11] L. Feeney, I.J. Harley, W.G. McCluggage, et al., World J. Clin. Oncol. 11 (2020) 868–889.
[12] R. McCorkle, J. Pasacreta, S.T. Tang, Holist. Nurs. Pract. 17 (2003) 300–308.
[13] N. Bharwani, R.H. Reznek, A.G. Rockall, Eur. J. Radiol. 78 (2011) 41–51.
[14] K.A. Kujawa, K.M. Lisowska, Postepy Hig. Med. Dosw. 69 (2015) 1275–1290.
[15] Z. Wang, F. Meng, Z. Zhong, Adv. Drug Deliv. Rev. 178 (2021) 13969–13981.
[16] T. Kaur, R.A. Slavcev, S.D. Wettig, Curr. Gene Ther. 9 (2009) 434–458.
[17] K. Itahana, J. Campisi, G.P. Dimri, Methods Mol. Biol. 371 (2007) 21–31.
[18] B.Y. Lee, J.A. Han, J.S. Im, et al., Aging Cell 5 (2006) 187–195.
[19] G. Jannone, M. Rozzi, M. Najimi, et al., J. Histochem. Cytochem. 68 (2020) 269–278.
[20] F. Fan, L. Zhang, X. Zhou, et al., J. Mater. Chem. B 9 (2021) 170–175.
[21] F. Mustafa, S. Liebich, S. Andreescu, Anal. Chim. Acta 1186 (2021) 39129–39137.
[22] P. Uruski, A. Sepetowska, C. Konieczna, et al., Cell. Mol. Biol. Lett. 26 (2021) 54–58.
[23] P. Uruski, J. Mikuła-Pietrasik, E. Naumowicz, et al., Biomedicines 9 (2021) 30–39.
[24] X. Li, Y. Pan, H. Chen, et al., Anal. Chem. 92 (2020) 5772–5779.
[25] L. Zhang, Y. Shan, X. Ji, et al., Oncotarget 8 (2017) 104745–104760.
[26] Y.Y. Shan, J.F. Wang, R. Si, et al., Bioorg. Chem. 108 (2021) 04551.
[27] P. Liang, X. Huang, Y. Wang, et al., ACS Nano 12 (2018) 11446–11457.
[28] Z. Zhou, H. Liang, R. Yang, et al., Angew. Chem. Int. Ed. 61 (2022) e202202843.